European Radiology
https://doi.org/10.1007/s00330-021-07732-0

NEURO

Simultaneously acquired PET and ASL imaging biomarkers may be helpful in differentiating progression from pseudo-progression in treated gliomas

Arnaud Pellerin[1,2] · Maya Khalifé[3,4] · Marc Sanson[5] · Laura Rozenblum-Beddok[6] · Marc Bertaux[6] · Marine Soret[6] · Damien Galanaud[2,3] · Didier Dormont[2] · Aurélie Kas[6,7] · Nadya Pyatigorskaya[2,3]

Received: 19 October 2020 / Revised: 21 December 2020 / Accepted: 29 January 2021

Abstract

Objectives The aim of this work was investigating the methods based on coupling cerebral perfusion (ASL) and amino acid metabolism ([^{18}F]DOPA-PET) measurements to evaluate the diagnostic performance of PET/MRI in glioma follow-up.

Methods Images were acquired using a 3-T PET/MR system, on a prospective cohort of patients addressed for possible glioma progression. Data were preprocessed with statistical parametric mapping (SPM), including registration on T1-weighted images, spatial and intensity normalization, and tumor segmentation. As index tests, tumor isocontour maps of [^{18}F]DOPA-PET and ASL T-maps were created and metabolic/perfusion abnormalities were evaluated with the asymmetry index *z*-score. SPM map analysis of significant size clusters and semi-quantitative PET and ASL map evaluation were performed and compared to the gold standard diagnosis. Lastly, ASL and PET topography of significant clusters was compared to that of the initial tumor.

Results Fifty-eight patients with unilateral treated glioma were included (34 progressions and 24 pseudo-progressions). The tumor isocontour maps and T-maps showed the highest specificity (100%) and sensitivity (94.1%) for ASL and [^{18}F]DOPA analysis, respectively. The sensitivity of qualitative SPM maps and semi-quantitative rCBF and rSUV analyses were the highest for glioblastoma.

Conclusion Tumor isocontour T-maps and combined analysis of CBF and [^{18}F]DOPA-PET uptake allow achieving high diagnostic performance in differentiating between progression and pseudo-progression in treated gliomas. The sensitivity is particularly high for glioblastomas.

Key Points

- *Applied separately, MRI and PET imaging modalities may be insufficient to characterize the brain glioma post-therapeutic profile.*
- *Combined ASL and [^{18}F]DOPA-PET map analysis allows differentiating between tumor progression and pseudo-progression.*

Keywords Prospective studies · Glioma · Magnetic resonance imaging · Perfusion, fluorodopa F 18

✉ Arnaud Pellerin
arnaudp76@hotmail.com

[1] Service de Neuroradiologie Diagnostique et Interventionnelle, Centre Hospitalier Universitaire de Nantes, Hôpital Nord Laennec, Rez-de-chaussée Bas Aile Est, Boulevard Jacques-Monod, Saint-Herblain, 44093 Nantes Cedex 1, France

[2] Service de Neuroradiologie Diagnostique et Fonctionnelle, Groupe Hospitalier Pitié-Salpêtrière C. Foix, 47-83 Boulevard de l'Hôpital, 75651 Paris Cedex 13, France

[3] Centre de NeuroImagerie de Recherche (CENIR), Institut du Cerveau et de la Moelle épinière (ICM), CNRS UMR 7225 – Inserm U1127 – Sorbonne Université – UMR S1127, 47-83 Boulevard de l'Hôpital, 75651 Paris Cedex 13, France

[4] Present address: Arterys, 34 av. des Champs-Elysées, 75008 Paris, France

[5] Service de Neurologie, Groupe Hospitalier Pitié-Salpêtrière C. Foix, 47-83 Boulevard de l'Hôpital, 75651 Paris Cedex 13, France

[6] Service de Médecine Nucléaire, Groupe Hospitalier Pitié-Salpêtrière C. Foix, 47-83 Boulevard de l'Hôpital, 75651 Paris Cedex 13, France

[7] Université Paris 6 UPMC, LIB Inserm U1146, 91-105 Boulevard de l'Hôpital, 75013 Paris, France

Published online: 31 March 2021

Abbreviations

[^{18}F]DOPA	^{18}F-Fluoro-3.4-dihydroxy-L-phenylalanine
[^{18}F]FDG	^{18}F-Fluoro-deoxy-glucose
ASL	Arterial spin labeling
CBF	Cerebral blood flow
CBV	Cerebral blood volume
DSC	Dynamic susceptibility contrast
FLAIR	Fluid-attenuated inversion recovery
FN	False negative
FP	False positive
MRI	Magnetic resonance imaging
pCASL	Pseudo-continuous spin-echo ASL
PET	Positron emission tomography
PWI	Perfusion-weighted imaging
rCBF	Cerebral blood flow ratio
rSUV	Standardized uptake value ratio
SE	Spin-echo
SPM	Statistical parametric mapping
SUV	Standardized uptake value
TN	True negative
TP	True positive
VOI	Volume of interest
WHO	World Health Organization
zAI	*Z*-score of the asymmetry index

Introduction

Surgery resection of adult brain glioma is often followed by adjuvant radiotherapy and/or chemotherapy [1]. However, complete remission, when occurs, is usually time-limited and the risk of tumor recurrence is high, especially for high-grade glial lesions [2].

MRI is the modality of choice for the glial tumor follow-up. Whenever new or increased contrast enhancement is detected [3], it is particularly important to distinguish between treatment-related necrosis and a recurrent tumor. However, it often appears difficult to do this with conventional MRI [4, 5], where contrast enhancement and FLAIR high-signal extension can be caused by physiological post-therapeutic blood-brain barrier disruption, radionecrosis, or pseudo-progression [6, 7].

In this context, advanced MRI and, in particular, perfusion-weighted MRI (PWI) can be helpful to detect neoangiogenesis, related to tumor progression. Dynamic susceptibility contrast (DSC)-PWI is now part of common tumor characterization and follow-up procedures [8, 9]. The alternatives to DSC-PWI in assessing cerebral blood flow (CBF) [10] are ASL-PWI and SE ASL, the latter technique being advantageous as it is less sensitive to post-therapeutic susceptibility artifacts. Nevertheless, the diagnostic performance of ASL-MRI remains imperfect [10].

[^{18}F]DOPA (18F-fluoro-3,4-dihydroxy-L-phenylalanine) PET is another imaging modality used to evaluate the post-therapeutic profile of brain tumors [11, 12]. However, in some patients, this method fails to unambiguously differentiate between viable tumor tissue and necrosis [13].

Thus, each of the above imaging modalities, used separately, may be insufficient in glioma follow-up.

Combined PET/MR offers the opportunity to acquire several biomarkers simultaneously. Simultaneous ASL-PWI and cerebral glucose metabolism investigation was first performed using [^{18}F]FDG-PET on MR-negative individuals with refractory focal epilepsy [14, 15]. The two techniques gave excellent concordance in the epilepsy focus localization. Morana et al [16] studied the diagnostic potential of ASL as compared to PET-CT in 26 pediatric astrocytic tumor. It was observed that combining ASL-CBF and [^{18}F]DOPA-PET SUV ratios increased the predictive power for prognosticating tumor progression suggesting a synergistic role of these diagnostic tools.

The aim of the present work was studying, in a reproducible quantitative way, cerebral perfusion measured by ASL-MRI and glucose metabolism measured by [^{18}F]DOPA-PET in post-therapeutic glioma to evaluate the potential of hybrid PET/MR in characterizing the tumor progression profile.

We expected that the proposed processing method of simultaneous analysis of ASL perfusion and [^{18}F]DOPA-PET maps will allow successful differentiation between tumor progression and treatment-related pseudo-progression or radionecrosis, bringing a robust method as an alternative to clinical routine standards.

Material and methods

Subjects

Consecutive patients, addressed for [^{18}F]DOPA-PET/MR follow-up examinations between December 2015 and January 2018 after brain tumor resection in our institution, were included. The patients with bilateral lesions or with obvious mass effect including the midline shift were excluded due to the chosen methodological approach. All data were extracted from the local prospective cohort of patients who underwent PET/MR, which was approved by the French authority for the protection of privacy and personal data in clinical research (CNIL, approval no. 2111722). This study was performed according to the principles of the Declaration of Helsinki.

Image acquisition

All images were acquired using an integrated PET/MR system (SIGNA PET/MR, GE Healthcare), according to the same

protocol, 10 min after the intravenous injection of 2 MBq/kg of [^{18}F]DOPA.

Simultaneous PET/MR acquisition was performed during 30 min, using an 8-channel head coil. The protocol included a 3D pseudo-continuous spin-echo ASL (pCASL) pulse sequence with the following parameters: echo time (TE) = 10.7 ms, repetition time (TR) = 4766 ms, post-label delay = 2025 ms, FOV = 240 × 240 mm^2, which resulted in the resolution of 1.875 × 1.875 × 4 mm^3. The CBF maps were calculated on the basis of the ASL images, using the perfusion quantification model [17]. The 3D T1 BRAVO images were acquired using the following parameters: TE = 3.8 ms, TR = 9.6 ms, flip angle = 15°, slice thickness = 1.4 mm, field of view (FOV) = 250 × 250 mm^2, 4 min after injecting gadoterate meglumine (Dotarem® 0.2 mL/kg, Guerbet).

PET images were reconstructed iteratively, using the ordered subset expectation maximization algorithm with 4 iterations and 28 subsets, including time of flight, point spread function, modeling and attenuation, truncation and scatter corrections, a reconstructed 256 × 256 image matrix, and in-plane Gaussian smoothing of FWHM = 3 mm, resulting in the reconstructed voxel size of 1.17 × 1.17 × 2.78 mm^3. For photon attenuation correction, the atlas-based method was implemented in the PET/MR system.

Statistical parametric mapping (SPM) pre-processing for voxel-wise comparison (flow diagram, Fig. 1)

All PET volumes and CBF maps were spatially normalized in the Montreal Neurological Institute (MNI) space, using SPM12 software (http://www.fil.ion.ucl.ac.uk/) by applying non-linear transformation, computed using co-registered T1-w volumes and an MNI template. This guarantees a reproducible analysis of imaging data and a similar reading plan. To avoid tumor spatial distortion during the normalization step, lesion masking was applied before computing the transformation matrix from the patient to the MNI space [18]. Tumor masks were obtained by manual segmentation on 3D T1 contrast-enhanced images, going beyond the enhanced lesion. The masks included FLAIR hyperintensity in close periphery since it was difficult to differentiate active tumor edema from gliosis. Once the transformation matrix is computed, the tumor masks were not used in the remainder of the processing pipeline. The transformation matrix from the lesion-masked T1 image to the MNI template was applied to both the PET image and the CBF map, both without any tumor masking. All the voxels in the normalized PET and ASL images held the initial image signal. The clusters as obtained are the existence of visually identifiable pixels characterized by a focal elevation of ASL perfusion and/or PET metabolism. The voxel size of the normalized PET and CBF images was 2 × 2 × 2 mm^3. A brain mask was created by thresholding the gray matter, the white matter, and the CSF tissue probability maps (TPM), available from SPM12, with subsequently merging all three masks. PET image intensity was normalized by scaling the voxel values of each individual image to the average SUV, measured in the VOI drawn on the contralateral healthy side of the parietal cortex. CBF intensity was normalized by the mean intensity of gray matter in the cerebellum. Three-dimensional smoothing of PET and CBF images was then performed with the Gaussian kernel of FWHM (full width at half maximum) equal to 10 mm and 8 mm, respectively. In order to find the best signal-to-noise ratio while investigating our 58 patients, without the loss of information, it appeared reasonable to use large smoothing filter to improve the signal detection and avoid artifacts.

Significant changes in lesion perfusion and metabolism were detected using voxel-wise comparison based on the single subject approach. As each selected patient had a lesion in one hemisphere only, the subject images were flipped so that a patient would have a lesion on the same side as in the control group. As a result, if a patient had a lesion in the left hemisphere, the control group included subjects with healthy left hemispheres.

Tumor perfusion (ASL-CBF) and metabolism (PET) were evaluated by voxel-wise comparison with the normal hemisphere. Using a 2-sample t test, a lesion PET image was compared with the normal-side PET image and the lesion CBF was compared with the normal-side CBF, which provided two corresponding SPM T-maps. Age and sex were set as covariates. For PET comparison, voxels were considered significant for $t > 6.36$, corresponding to $p < 0.05$ corrected by the family-wise error (FWE) method at the voxel level without the minimal cluster size. For ASL comparison, the significance threshold was set at $t > 3.25$, corresponding to $p < 0.001$ without correction for FWE. T-value isocontour maps of PET and ASL T-maps were created for $t \geq 6.36$ and $t \geq 3.25$, respectively. Next, the significant voxels obtained were normalized by the tumor size and compared to our reference standard, obtained in the follow-up of histological confirmation.

Evaluation of metabolic/perfusion abnormalities using the asymmetry index (AI)

The asymmetry index z-score (zAI) was applied to ASL and PET for depicting significant differences between each tumor side and the normal contralateral side. For each patient, CBF and rSUV maps were computed to obtain the voxel-wise AI value: AI = 100 * [right − left] / [(right + left) / 2].

The AI value was calculated for each voxel, positive values corresponding to the right->left side control population [14, 19]. After calculating the mean (μ_{AI}) and the standard deviation (SD_{AI}) of the whole set of AI values, the voxel-wise AI z-score map was derived: zAI = (AI − μ_{AI}) / SD_{AI}.

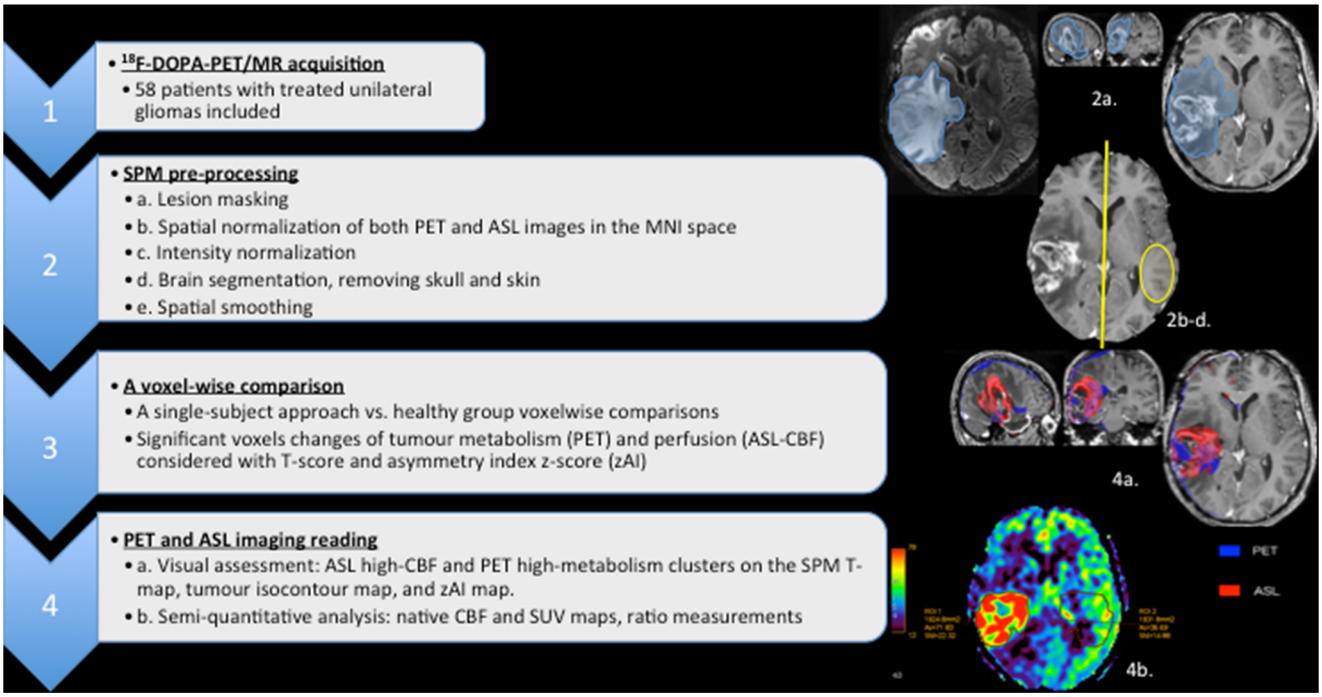

Fig. 1 Flow diagram of imaging processing and analysis. SPM statistical parametric mapping software, MNI Montreal Neurological Institute space

Assuming normal distribution, voxels with $|zAI| \geq 1.64$ and $p < 0.05$ were considered to have significantly different rSUV or CBF values for the two hemispheres. For visualization purposes, brain voxels with statistically significant rSUV/CBF asymmetry were displayed on the right hemisphere if $zAI \leq -1.64$ (right < left) and on the left hemisphere if $zAI \geq 1.64$ (right > left).

Consequently, for each patient, five maps were created: native CBF and SUV maps, ASL high-CBF and PET high-metabolism clusters on the T-map, the tumor isocontour map, and the zAI map (Figs. 2, 3, 4, and 5). Visual assessment of the last three parameters, obtained with SPM, is further referred to as index tests.

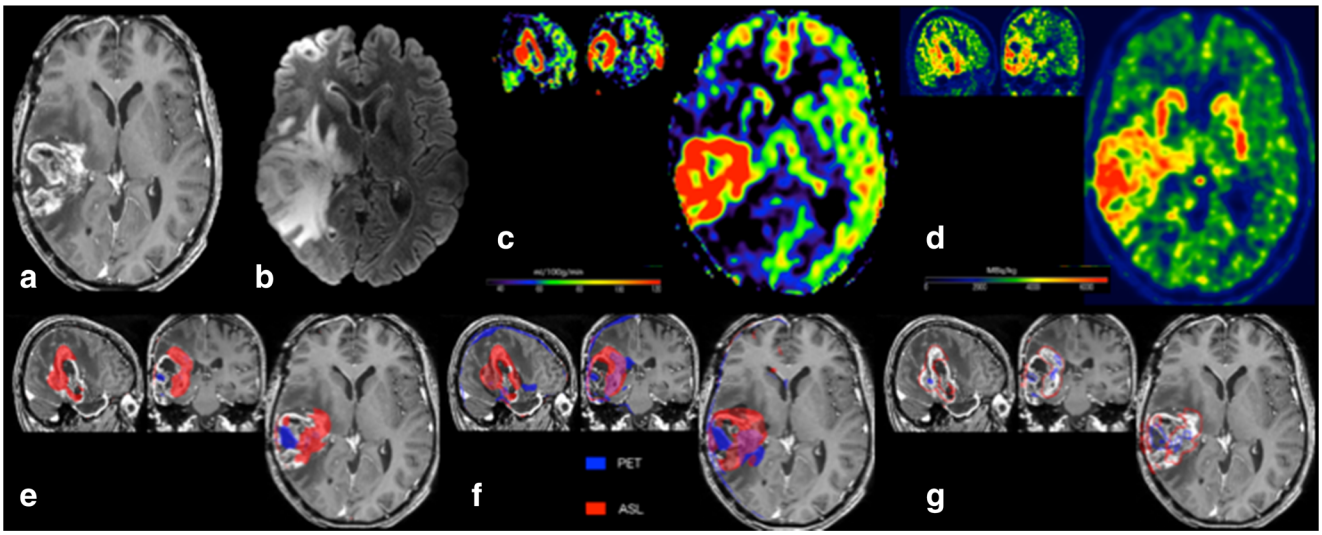

Fig. 2 PET-MR of a 44-year-old female patient with a right-sided glioblastoma WHO IV without IDH mutation, treated by surgery and adjuvant radio-chemotherapy. The tumor progression was confirmed by the follow-up (true positive for ASL and PET). Upper row: **a** Enhancement at the initially treated parietal tumor site on a contrast-enhanced axial T1-w image. **b** Axial FLAIR-w image. **c** Hyper-perfusion with increased CBF on ASL images (rCBF: 2.0) corresponds to the area of contrast enhancement. **d** [^{18}F]DOPA-PET map with increased SUV (SUV max: 4.9, rSUV: 1.2). Lower row: The SPM maps were concordant with the positive clusters, confirming progression (blue and red signals for PET and ASL, respectively). **e** *T*-score map. **f** *Z*-score of asymmetry index. **g** Isocontour map

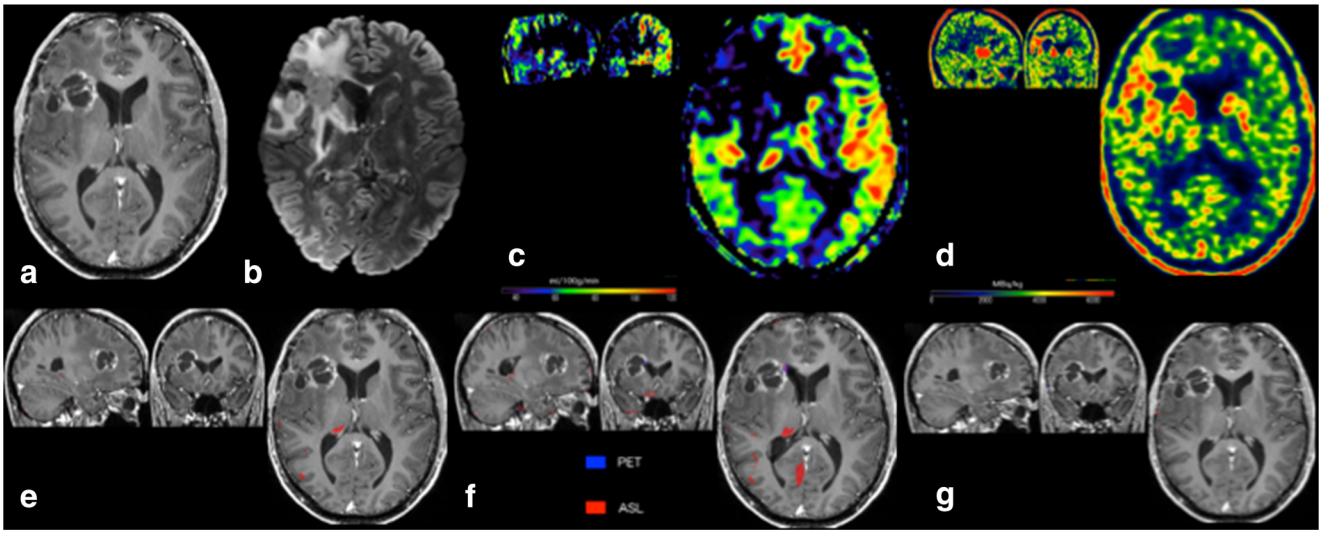

Fig. 3 PET-MR of a 40-year-old male patient with a right-sided glioblastoma WHO IV with IDH mutation, treated by surgery and adjuvant radiotherapy. Pseudo-progression was confirmed by the follow-up (true negative for ASL and PET). Upper row: **a** Linear cavitary enhancement observed at the initially treated frontal lesion site on a contrast-enhanced axial T1-w image. **b** Axial FLAIR-w image. **c** The absence of hyper-perfusion as assessed by CBF on ASL images (rCBF: 0.58). **d** A [^{18}F]DOPA-PET map showing no significantly increased SUV (SUV max: 2.5, rSUV: 0.9). Lower row: The SPM maps were concordant and no significant clusters at the tumor site were observed, which confirmed pseudo-progression, while the standard clinical analysis may be difficult given the limit value of rSUV close to 1. **e** *T*-score map. **f** *Z*-score of asymmetry index. **g** Isocontour map

Semi-quantitative image analysis

PET/MR images were analyzed by 2 radiologists (A.P. and N.P.) and 2 nuclear medicine physicians (A.P. and N.P.). The raters were blinded to the previous patients' medical history, pathological findings, and other imaging modalities. The images were analyzed using the Advantage Workstation 4.6 (GE Healthcare). The raters manually drew ROIs at the tumor site on the CBF maps and the SUV images in the suspected area. To calculate the rCBF and rSUV, the reference ROI was defined on the contralateral healthy hemisphere and in the contralateral striatum, respectively.

Firstly, for both imaging modalities, each patient was semi-quantitatively classified on the basis of the rCBF and rSUV

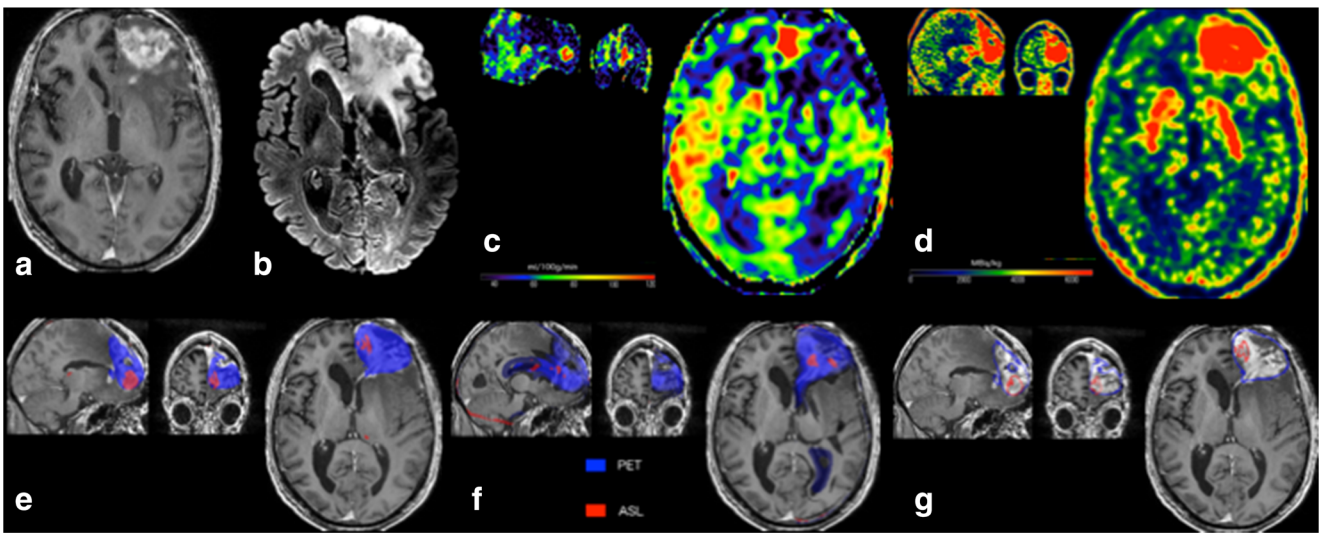

Fig. 4 PET-MR of a 70-year-old male patient with a left-sided WHO IV glioblastoma without IDH mutation, treated by surgery and adjuvant radio-chemotherapy. Tumor progression was confirmed by the follow-up (true positive for ASL and PET). Upper row: **a** Enhancement at the initially treated frontal lesion site on a contrast-enhanced axial T1-w image. **b** Axial FLAIR-w image. **c** Hyper-perfusion with increased CBF on the ASL images (rCBF: 2.4) corresponds to the area of contrast enhancement. **d** A [^{18}F]DOPA-PET map with increased SUV (SUV max: 3.8, rSUV: 1.5). Lower row: The SPM maps were concordant with significant clusters, which confirmed the tumor progression. The red ASL clusters appear to be more peripheral than the blue extensive PET clusters. **e** *T*-score map. **f** *Z*-score of asymmetry index. **g** Isocontour map

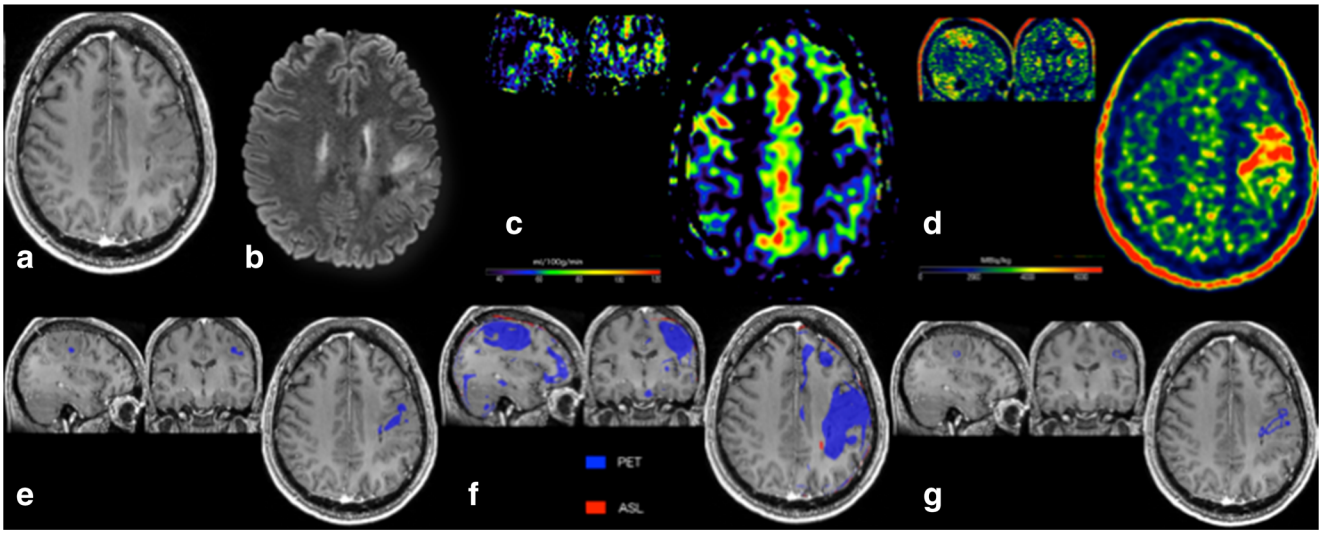

Fig. 5 PET-MR of a 49-year-old male patient with a left-sided WHO III oligodendroglioma with IDH mutation and 1p/19q co-deletion, treated by radio-chemotherapy after biopsy. Tumor pseudo-progression was confirmed by the follow-up (true negative for ASL and false positive for PET). Upper row: **a** The absence of contrast enhancement at the initially treated frontal lesion site on a contrast-enhanced axial T1-w image. **b** Axial FLAIR-w image. **c** No significant hyper-perfusion on a CBF ASL map (rCBF: 0.94). **d** A [^{18}F]DOPA-PET map with increased SUV (SUV max: 4.2, rSUV: 1.4). Lower row: The SPM maps were discordant with significant PET clusters, but no ASL clusters were observed at the tumor site. **e** A *T*-score map. **f** *Z*-score of asymmetry index. **g** An isocontour map

ratios, used as index tests. In the case of [^{18}F]DOPA-PET, the readers used the threshold rSUV higher than 1.0 and 2.0 for the striatum and the contralateral cortex, respectively [20]. The images that suggested the tumor recurrence or progression were considered pathological and scored 1; the ratios ≤ 1 were considered pseudo-progression or radionecrosis and scored 0.

Secondly, an NIfTI format image viewer (Chris Rorden's MRIcron software, http://people.cas.sc.edu/rorden/mricron/install.html) was employed to visually assess the *T*-score, tumor isocontour, and *z*AI maps generated using SPM. The neuroimaging readers classified significant cluster sizes found on morphological T1 images by the same rating as the native CBF and PET readings (Figs. 2, 3, 4, and 5).

Diagnostic confirmation

The initial diagnosis for all patients was made on the basis of the histological analysis of the cerebral biopsy or the initial surgery results (Table 1) [21, 22]. Progression or pseudo-progression was established by the reference standard, including histological confirmation when MRI was followed by biopsy or resection or by the follow-up for at least 3 or 9 months without treatment modification for high- and low-grade gliomas, respectively. The PET-MRI results were not used in the establishment of the gold standard diagnosis.

Statistical analysis

The results of the analysis of each SPM map as well as of the CBF and PET readings were compared to the gold standard diagnosis. Sensitivity, specificity, PPV, and NPV were calculated. The subgroup analyses for low- and high-grade and for WHO III and WHO IV tumors were performed.

Additionally, qualitative analysis of the SPM maps was performed to assess the PET and CBF high-signal cluster topography.

Results

Patients and lesions (Table 1)

Fifty-eight patients (mean age 53.1 ± 14.3, 34 males) with treated unilateral gliomas who were included in the study constituted a group of 10 (17.2%) low-grade and 48 (82.8%) high-grade gliomas. The patients' clinical characteristics are shown in Table 1.

Contrast enhancement

Eight patients with radionecrotic lesions or pseudo-progression (3 low- and 5 high-grade gliomas) presented no contrast enhancement (13.8%).

Contrast enhancement was observed in 50 patients (86.2%), 16 cases corresponding to radionecrotic lesions or pseudo-progression (32%) and 34 cases corresponding to progression (68%: 7 low- (14%) and 43 high-grade (86%) lesions).

Table 1 Patient's clinical characteristics

		Patients (n = 58)
Sex		
Women (n (%))		24 (41.4%)
Men (n (%))		34 (58.6%)
Age (years)		
Mean		53.1
STD		14.3
WHO glioma grade (n (%))		
I		0 (0%)
II		10 (17.2%)
III		21 (36.2%)
IV		27 (46.6%)
Biology molecular alterations		
IDH1/2 mutations		43 (74.1%)
Wild-type		15 (25.9%)
1p/19q co-deletion		9 (15.5%)
Lateralization of tumor		
Right		25 (43.1%)
Left		33 (56.9%)
Initial biopsy or surgery		
Biopsy		20 (34.5%)
Surgery		38 (65.5%)
Adjuvant radiotherapy and/or chemotherapy		
Radiotherapy		52 (89.7%)
Chemotherapy		43 (74.1%)
Radiotherapy and chemotherapy		39 (67.2%)
None		2 (3.4%)
Follow-up clinical reference status (gold standard)		
Pseudo-progression and radionecrotic lesions	All lesions	24 (41.4%)
	WHO III	10 (47.6%)
	WHO IV	7 (25.9%)
Progression	All lesions	34 (58.6%)
	WHO III	11 (52.4%)
	WHO IV	20 (74.1%)

STD standard deviation, *WHO* World Health Organization, *IDH* isocitrate dehydrogenase mutation

Semi-quantitative PET and CBF map analysis (Table 2)

In patients with progression, [^{18}F]DOPA-PET images showed significant hyper-metabolism in 32/34 patients (94.1%), including 3/3 patients (100%) with low-grade and 29/31 patients (93.5%) with high-grade gliomas. The overall sensitivity and specificity were 94.1% and 79.2%, respectively (true positive (TP): 32 patients; false positive (FP): 5 patients).

ASL images showed significant hyper-perfusion in 22/34 patients (64.7%) with progression, including 1/3 patient (33.3%) with low-grade and 21/31 patients (67.7%) with high-grade gliomas. The sensitivity and specificity were 64.7% and 100%, respectively (TP: 22; FP: 0).

ROC curves with AUC obtained by semi-quantitative analysis are shown in Fig. 6.

Qualitative SPM map analysis (Table 2)

*z*AI maps

A pathological cluster was revealed in the PET *z*AI maps of each patient (34/34) with the final diagnosis of progression, the overall sensitivity and specificity being 100% and 58.3%, respectively (TP: 34; FP: 0). The ASL *z*AI maps showed significant clusters in 19 patients with progression (55.9%), thus the sensitivity and specificity of this sequence being 55.9% and 87.8%, respectively (TP: 19; FP: 3).

Isocontour maps

The PET isocontour maps showed significant clusters at the tumor site in 32/34 patients (94.1%) with progression. Thus, in this case, the sensitivity and specificity were 94.1% and 91.7%, respectively, for all glioma grades involved (TP: 32; FP: 2). The ASL isocontour maps showed significant clusters at the tumor site in 21/34 patients (61.8%) for all glioma grades, the sensitivity and specificity being 61.8% and 100%, respectively (TP: 21; FP: 0).

The above statistical results were similar to those obtained from the PET and ASL T-maps.

Assessment of ASL and PET cluster topography (Table 3)

When clusters were observed on the pathological hemispheres, they were, in most cases, located inside the lesion (within the enhancement regions or the FLAIR hyperintensity regions) or on the lesion periphery for both PET (86.3%) and ASL (64.7%). The location inside the lesion was observed more often in the case of progression (78.8%) than in the case of pseudo-progression (21.2%).

The topography of high ASL-CBF and PET metabolism clusters for the three SPM maps was assessed. The analysis of ASL and PET cluster overlaying has shown 51.5% with < 33% of overlaying voxels and 27.3% with > 66% of overlaying voxels, respectively.

Clusters of high ASL-CBF were located within the PET clusters in 61.8% of cases of progression. The location was, in most cases (64.3%), on the lesion periphery.

Table 2 Evaluation of sensitivity, specificity, positive predictive value (PPV), and negative predictive value (NPV) of the qualitative analysis using SPM maps, and of the semi-quantitative analysis using CBF and SUV maps. The reference standard includes histological confirmation when MRI was followed by biopsy or resection or by clinical and imaging follow-up

			Sensitivity (%)	Specificity (%)	PPV (%)	NPV (%)	TP (*n*)	TN (*n*)	FP (*n*)	FN (*n*)	Total (*n*)
Qualitative analysis using SPM maps	T-map and isocontour map ASL	All	61.8	100	100	64.9	21	24	0	13	58
		Low-grade	33.3	100	100	77.8	1	7	0	2	10
		High-grade	64.5	100	100	60.7	20	17	0	11	48
	T-map and isocontour map PET	All	94.1	91.7	94.1	91.7	32	22	2	2	58
		Low-grade	100	100	100	100	3	7	0	0	10
		High-grade	93.5	88.2	93.5	88.2	29	15	2	2	48
	*z*AI map ASL	All	55.9	87.5	86.4	58.3	19	21	3	15	58
		Low-grade	33.3	85.7	50	75	1	6	1	2	10
		High-grade	58.1	88.2	90	53.6	18	15	2	13	48
	*z*AI map PET	All	100	58.3	77.3	100	34	14	10	0	58
		Low-grade	100	57.1	50	100	3	4	3	0	10
		High-grade	100	58.8	81.6	100	31	10	7	0	48
Semi-quantitative analysis using CBF and SUV maps	CBF ASL analysis	All	64.7	100	100	66.7	22	24	0	12	58
		Low-grade	33.3	100	100	77.8	1	7	0	2	10
		High-grade	67.8	100	100	63	21	17	0	10	48
	SUV PET analysis	All	94.1	79.2	86.5	90.5	32	19	5	2	58
		Low-grade	100	71.4	60	100	3	5	2	0	10
		High-grade	93.5	82.4	90.6	87.5	29	14	3	2	48
High-grade lesions; qualitative analysis using SPM maps	T-map and isocontour map ASL	WHO III	27.3	100	100	55.6	3	10	0	8	21
		WHO IV	85	100	100	70	17	7	0	3	27
	T-map and isocontour map PET	WHO III	90.9	90	90.9	90	10	9	1	1	21
		WHO IV	95	85.7	95	85.7	19	6	1	1	27
	*z*AI map ASL	WHO III	36.4	90	80	56.3	4	9	1	7	21
		WHO IV	70	85.7	93.3	50	14	6	1	6	27
	*z*AI map PET	WHO III	100	60	73.3	100	11	6	4	0	21
		WHO IV	100	57.1	87	100	20	4	3	0	27
High-grade lesions; semi-quantitative analysis with CBF and SUV maps	CBF ASL analysis	WHO III	36.4	100	100	58.8	4	10	0	7	21
		WHO IV	85	100	100	70	17	7	0	3	27
	SUV PET analysis	WHO III	90.9	90	90.9	90	10	9	1	1	21
		WHO IV	95	71.4	90.5	83.3	19	5	2	1	27

ASL arterial spin labeling, *CBF* cerebral blood flow, *PET* positron emission tomography, *SPM* statistical parametric mapping, *SUV* standardized uptake value, *WHO* World Health Organization, *zAI* *z*-score of the asymmetry index, *TP* true positive, *TN* true negative, *FP* false positive, *FN* false negative

Discussion

In the present work, we propose an objective method of simultaneous analysis of ASL perfusion and [^{18}F]DOPA-PET maps for the evaluation of glial tumor progression (Fig. 2). Tumoral isocontour and T-map analyses have shown high diagnostic accuracy with the highest specificity for ASL-CBF analysis and the highest sensitivity for [^{18}F]DOPA analysis, which suggests that these two biomarkers, acquired during the same examination session, are concordant and complementary.

The contrast enhancement that corresponds to the blood-brain barrier disruption can originate not only from tumor progression but also from post-surgery modifications, radionecrosis, or chemotherapy [23]. Consequently, there is a need for more specific analysis of the tumor tissue, which can be done by advanced MRI techniques, such as perfusion, and also by PET metabolic imaging.

Regarding perfusion techniques, in this study, we chose the pCASL perfusion modality to investigate tumor neoangiogenesis [24]. This SE sequence is advantageous to DSC-PWI since it is known to reduce susceptibility artifacts

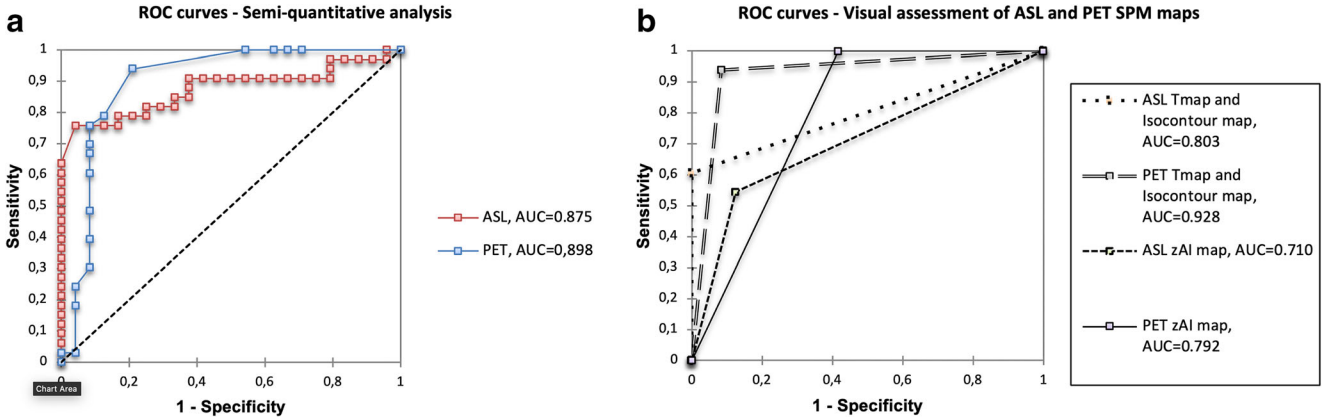

Fig. 6 ROC curves with AUC obtained by (**a**) semi-quantitative analysis: ASL and PET imaging using CBF and SUV ratio measurements respectively. **b** Visual assessment of SPM T-map, isocontour map, and *z*AI map. The dotted line is the reference line. ROC receiver operating curve, AUC area under the curve

[25], which is particularly crucial around the resection cavities, where blood products can affect the DSC results [26] (Fig. 2). In addition, ASL is less sensitive to the presence of the surrounding vessels, which is often the issue in primary brain tumor lesions [10]. This sequence was shown to be a reliable alternative in the evaluation of tumor perfusion and glioma grade [11, 27, 28]. ASL is of particular interest in the case of gadolinium-based perfusion being contraindicated [10]. Moreover, for a wide range of gliomas, CBF has proved to provide better quantitative estimation of event-free survival than a histologic grading scale does [29]. Our results suggest that the CBF significant cluster size decreases in the case of tumor pseudo-progression (Fig. 3), which can be explained by the absence of neoangiogenesis and/or by the presence of necrosis, usually observed after radiotherapy. In contrast to this, the CBF cluster size increased in most cases of progression.

The use of [^{18}F]FDG-PET in brain tumor metabolic imaging is limited by the increased uptake in normal brain tissue and by nonspecific uptake in inflammatory benign lesions [30]. Amino acid tracers, including [^{18}F]DOPA-PET, were most successful in this field [31].

In the present study, we have demonstrated the advantage of analyzing both [^{18}F]DOPA-PET uptake and ASL maps, the former being highly sensitive and the latter highly specific for WHO III and IV gliomas. We have also studied the relationship between the blood-brain barrier distribution as observed by contrast enhancement and the lesion neoangiogenesis as analyzed by ASL data and the lesion metabolism evaluated by PET imaging. We have shown that, when contrast

Table 3 Qualitative assessment of ASL and PET cluster topography on the basis of SPM maps

	T-map	*z*AI map	Isocontour map
ASL and PET clusters of voxel overlaying (*n* patients)			
No overlaying or absence of ASL cluster	38	32	38
< 33%	10	14	10
33–66%	5	4	5
> 66%	5	8	5
Total	58	58	58
ASL cluster topography related to PET (*n* patients)			
1- Perfect overlaying	1	0	1
2- Central	7	8	8
3- Deep peripheric	8	9	7
4- Peripheric	6	9	6
5- Unsystematized	3	7	1
6- Outside	3	10	4
7- Absence	30	15	31
Total	58	58	58

enhancement is observed, it is most frequently concordant with the qualitative assessment of ASL and PET cluster topography based on the SPM maps. Significant clusters are, in most cases (80.4%), located inside contrast-enhancing lesions or on their periphery (Fig. 4) for both PET and ASL. The finding of the PET clusters being more expanded than the ASL ones (Fig. 4) can be explained by more extensive metabolism and more localized neoangiogenesis. We have observed that the ASL clusters are more often located on the lesion periphery (64.3%), especially in the case of high-grade tumor progression (Fig. 4), which suggests preferential neoangiogenesis on the tumor periphery [32]. It is also known that amino acid uptake usually extends beyond the contrast-enhanced T1-w abnormalities [33].

In a few cases, we encountered discordance between the PET and ASL SPM maps. The true negative ASL cases could be related to pseudo-progression (Fig. 5), while the false negative (FN) ASL cases could be accounted for by various reasons. Twelve FN ASL cases were observed using semi-quantitative analysis as compared to 2 FN results obtained by PET. The FN results were caused by the tumor proximity to the cranial vault or by the small size of the clusters located close to the cortical vessels. Since the diagnostic performance, especially for the CBF maps, appears to be lower for WHO III tumors, further studies on these lesions are required. Five FP PET and no FP ASL cases were observed. Thus, the ASL analysis being combined with PET provides good diagnostic accuracy in glioma evaluation.

The analysis in clinical practice is usually performed visually or semi-quantitatively, on native images [34, 35]. However, for large population clinical trials, a quantitative, robust, reproducible, and standardized method should be developed. Such methods are, currently, becoming particularly crucial for integrating artificial intelligence in image analysis. The analysis proposed in this paper provides similar or better results as compared to standard readings; it is objective and easy to adopt by users with modest experience.

Our study has several limitations. Firstly, the contralateral side of the patients' brain used for the comparison with that of the "healthy" group could also been exposed to radiotherapy and chemotherapy. However, similar methodology of considering only one side of the brain to be modified by the disease was also previously used [14]. Moreover, all the subjects were thoroughly checked in order to ensure the absence of pathology on the contralateral side. Secondly, in our sample, the number of progressions was higher than that of pseudo-progressions (Table 1), in line with the clinical workflow and the natural history of the disease, since the majority of the lesions were high-grade glioma (82.8%).

In summary, the present work proposes a robust, objective method of simultaneous analysis of ASL perfusion and [^{18}F]DOPA-PET maps for the evaluation of glial tumor progression. Simultaneous analysis of the tumor CBF isocontour and T-maps and the [^{18}F]DOPA-PET uptake allows achieving high diagnostic performance. This can help differentiate between tumor progression and pseudo-progression or radionecrosis. The method can be promising for large-scale clinical trials and artificial intelligence studies, where unbiased reproducible techniques are required.

Funding The authors state that this work has not received any funding.

Compliance with ethical standards

Guarantor The scientific guarantor of this publication is Arnaud Pellerin, the corresponding author.

Conflict of interest The authors of this manuscript declare relationships with the following company:

Maya Khalifé received a research grant from General Electric Healthcare. No other financial relationships that might lead to a perceived conflict of interest relevant to this article were reported.

Statistics and biometry One of the authors has significant statistical expertise.

No complex statistical methods were necessary for this paper.

Informed consent Written informed consent was not required for this study. All data were extracted from the local database of PET/MR studies, which was approved by the French authority for the protection of privacy and personal data in clinical research (CNIL, No. 2111722). This study was performed according to the principles of the Declaration of Helsinki.

Ethical approval Institutional Review Board approval was obtained.

Methodology
- prospective
- case-control study/observational
- performed at one institution

References

1. Ricard D, Idbaih A, Ducray F, Lahutte M, Hoang-Xuan K, Delattre JY (2012) Primary brain tumours in adults. Lancet Lond Engl 379: 1984–1996
2. Klobukowski L, Falkov A, Chelimo C, Fogh SE (2018) A retrospective review of re-irradiating patients' recurrent high-grade gliomas. Clin Oncol (R Coll Radiol). https://doi.org/10.1016/j.clon.2018.05.004
3. Thust SC, Heiland S, Falini A et al (2018) Glioma imaging in Europe: a survey of 220 centres and recommendations for best clinical practice. Eur Radiol 28:3306–3317
4. Kumar AJ, Leeds NE, Fuller GN et al (2000) Malignant gliomas: MR imaging spectrum of radiation therapy- and chemotherapy-induced necrosis of the brain after treatment. Radiology 217:377–384
5. Mullins ME, Barest GD, Schaefer PW et al (2005) Radiation necrosis versus glioma recurrence: conventional MR imaging clues to diagnosis. AJNR Am J Neuroradiol 26:1967–1972

6. Aronen HJ, Gazit IE, Louis DN et al (1994) Cerebral blood volume maps of gliomas: comparison with tumor grade and histologic findings. Radiology 191:41–51
7. Law M, Yang S, Wang H et al (2003) Glioma grading: sensitivity, specificity, and predictive values of perfusion MR imaging and proton MR spectroscopic imaging compared with conventional MR imaging. AJNR Am J Neuroradiol 24:1989–1998
8. Mabray MC, Barajas RF, Cha S (2015) Modern brain tumor imaging. Brain Tumor Res Treat 3:8–23
9. Rossi A, Gandolfo C, Morana G, Severino M, Garrè ML, Cama A (2010) New MR sequences (diffusion, perfusion, spectroscopy) in brain tumours. Pediatr Radiol 40:999–1009
10. Haller S, Zaharchuk G, Thomas DL, Lovblad KO, Barkhof F, Golay X (2016) Arterial spin labeling perfusion of the brain: emerging clinical applications. Radiology 281:337–356
11. Galldiks N, Stoffels G, Ruge MI et al (2013) Role of O-(2-18F-fluoroethyl)-L-tyrosine PET as a diagnostic tool for detection of malignant progression in patients with low-grade glioma. J Nucl Med 54:2046–2054
12. Pirotte BJM, Levivier M, Goldman S et al (2009) Positron emission tomography-guided volumetric resection of supratentorial high-grade gliomas: a survival analysis in 66 consecutive patients. Neurosurgery 64:471–481 discussion 481
13. Brandes AA, Tosoni A, Spagnolli F et al (2008) Disease progression or pseudoprogression after concomitant radiochemotherapy treatment: pitfalls in neurooncology. Neuro Oncol 10:361–367
14. Boscolo Galazzo I, Mattoli MV, Pizzini FB et al (2016) Cerebral metabolism and perfusion in MR-negative individuals with refractory focal epilepsy assessed by simultaneous acquisition of (18)F-FDG PET and arterial spin labeling. Neuroimage Clin 11:648–657
15. Storti SF, Boscolo Galazzo I, Del Felice A et al (2014) Combining ESI, ASL and PET for quantitative assessment of drug-resistant focal epilepsy. Neuroimage 102(Pt 1):49–59
16. Morana G, Piccardo A, Tortora D et al (2017) Grading and outcome prediction of pediatric diffuse astrocytic tumors with diffusion and arterial spin labeling perfusion MRI in comparison with 18F-DOPA PET. Eur J Nucl Med Mol Imaging 44:2084–2093
17. Alsop DC, Detre JA, Golay X et al (2015) Recommended implementation of arterial spin-labeled perfusion MRI for clinical applications: a consensus of the ISMRM perfusion study group and the European consortium for ASL in dementia. Magn Reson Med 73:102–116
18. Brett M, Leff AP, Rorden C, Ashburner J (2001) Spatial normalization of brain images with focal lesions using cost function masking. Neuroimage 14:486–500
19. Lim Y-M, Cho Y-W, Shamim S et al (2008) Usefulness of pulsed arterial spin labeling MR imaging in mesial temporal lobe epilepsy. Epilepsy Res 82:183–189
20. Chen W, Silverman DHS, Delaloye S et al (2006) 18F-FDOPA PET imaging of brain tumors: comparison study with 18F-FDG PET and evaluation of diagnostic accuracy. J Nucl Med 47:904–911
21. Louis DN, Ohgaki H, Wiestler OD et al (2007) The 2007 WHO classification of tumours of the central nervous system. Acta Neuropathol 114:97–109
22. Komori T (2017) The 2016 WHO classification of tumours of the central nervous system: the major points of revision. Neurol Med Chir (Tokyo) 57:301–311
23. Bergamino M, Saitta L, Barletta L et al (2013) Measurement of blood-brain barrier permeability with t1-weighted dynamic contrast-enhanced MRI in brain tumors: a comparative study with two different algorithms. ISRN Neurosci 2013:905279
24. Dolui S, Vidorreta M, Wang Z et al (2017) Comparison of PASL, PCASL, and background-suppressed 3D PCASL in mild cognitive impairment. Hum Brain Mapp 38:5260–5273
25. Gai ND, Chou YY, Pham D, Butman JA (2017) Reduced distortion artifact whole brain CBF mapping using blip-reversed non-segmented 3D echo planar imaging with pseudo-continuous arterial spin labeling. Magn Reson Imaging 44:119–124
26. Lindner T, Ahmeti H, Juhasz J et al (2018) A comparison of arterial spin labeling and dynamic susceptibility perfusion imaging for resection control in glioblastoma surgery. Oncotarget 9:18570–18577
27. Galldiks N, Langen K-J, Holy R et al (2012) Assessment of treatment response in patients with glioblastoma using O-(2-18F-fluoroethyl)-L-tyrosine PET in comparison to MRI. J Nucl Med 53:1048–1057
28. Pafundi DH, Laack NN, Youland RS et al (2013) Biopsy validation of 18F-DOPA PET and biodistribution in gliomas for neurosurgical planning and radiotherapy target delineation: results of a prospective pilot study. Neuro Oncol 15:1058–1067
29. Furtner J, Bender B, Braun C et al (2014) Prognostic value of blood flow measurements using arterial spin labeling in gliomas. PLoS One 9:e99616
30. Salber D, Stoffels G, Pauleit D et al (2007) Differential uptake of O-(2-18F-fluoroethyl)-L-tyrosine, L-3H-methionine, and 3H-deoxyglucose in brain abscesses. J Nucl Med 48:2056–2062
31. Langen K-J, Bröer S (2004) Molecular transport mechanisms of radiolabeled amino acids for PET and SPECT. J Nucl Med 45:1435–1436
32. Gasparetto EL, Pawlak MA, Patel SH et al (2009) Posttreatment recurrence of malignant brain neoplasm: accuracy of relative cerebral blood volume fraction in discriminating low from high malignant histologic volume fraction. Radiology 250:887–896
33. Filss CP, Cicone F, Shah NJ, Galldiks N, Langen K-J (2017) Amino acid PET and MR perfusion imaging in brain tumours. Clin Transl Imaging 5:209–223
34. Wang Y-F, Hou B, Yang S-J et al (2016) Diagnostic significance of arterial spin labeling in the assessment of tumor grade in brain. J Cancer Res Ther 12:259–266
35. Kinahan PE, Fletcher JW (2010) Positron emission tomography-computed tomography standardized uptake values in clinical practice and assessing response to therapy. Semin Ultrasound CT MR 31:496–505